

# We are IntechOpen, the world's leading publisher of Open Access books Built by scientists, for scientists

6,900

Open access books available

186,000

International authors and editors

200M

Downloads

Our authors are among the

154

Countries delivered to

TOP 1%

most cited scientists

12.2%

Contributors from top 500 universities



WEB OF SCIENCE™

Selection of our books indexed in the Book Citation Index  
in Web of Science™ Core Collection (BKCI)

Interested in publishing with us?  
Contact [book.department@intechopen.com](mailto:book.department@intechopen.com)

Numbers displayed above are based on latest data collected.  
For more information visit [www.intechopen.com](http://www.intechopen.com)



# Reconfigurable Filter Design

*Tae-Hak Lee, Sang-Gyu Lee, Jean-Jacques Laurin and Ke Wu*

## Abstract

This chapter discusses recent development of reconfigurable filters. The technical terminology reconfigurable means that a circuit is designed in a way to have various electrical characteristics comparing with one which has a static feature. For the filter design, the various electrical characteristics can be considered as the filter can tune its operating frequency, bandwidth, and/or have multiple operational modes, that is, bandstop or bandpass modes. Also, recently, the filters that can exhibit an improved impedance matching performance over its stopband have been reported. It provides more options for the filter designers to realize the reconfigurable filters having reflective and/or absorptive frequency response types to satisfy a prior given requirement. In this chapter, recently devised filter designs will be covered and essential frequency tuning elements to realize the reconfigurable characteristic will be introduced as well.

**Keywords:** resonant frequency, operational modes, reflective, absorptive, frequency tuning elements

## 1. Introduction

Microwave filters play an important role in the chain of radio frequency (RF) front end to transmit and receive the required signals or to block the undesired ones. Most filter designs are dependent on the electrical length of the operating frequency or the field configuration of the resonant modes inside a cavity so the reconfigurable characteristic such as the capability to tune the operating frequency, bandwidth, and operational modes can be obtained by controlling the dependent design parameters. Recently, some researchers embarked on the development of filters that have the better matching performance at its stopband region to avoid using the isolators. The improved impedance matching characteristic is achieved in a way the input signal not to be reflected back to the input port by absorbing the input signal inside the filter structure so the devised circuits having the improved impedance performance are often named as an absorptive or a reflectionless filter.

In this chapter, we will explore the recent development of reconfigurable filter designs that can change their operating frequency, bandwidth, and operational modes along with some tuning components. Besides, the filter designed to have both reflective and absorptive characteristics will be shown. The frequency tunable substrate integrated waveguide (SIW) resonators are used to change the operating frequency of the reconfigurable filter and, to achieve frequency agility, the tuning elements based on the piezoelectric disk or the electromagnet are also given. To verify the tuning method using the electromagnet, frequency tunable filtering balun is fabricated and tested using four electromagnets. In the following section, we first start from the theoretical modelings of the frequency responses of the

reconfigurable filter using coupling coefficients and equivalent circuits, and then the circuit model with simulation and measurement results are given to support the theoretical modelings.

## 2. Filter designs

The coupling coefficients and their array in form of a matrix containing the inverter values are widely used to explain or represent the operation mechanism of the filter structure. The fundamental theory and detailed concepts to establish the coupling coefficients and matrix can be found from well-known textbooks [1, 2]. In this section, we will briefly cover the definition of two coupling coefficients and the experimental process to assess the coupling coefficients of the physical external, or inter-resonator coupling structures. Both couplings essentially need to be defined for the theoretical frequency responses and the associated coefficient to each coupling structure should be realized from the coupling structures for the filter to satisfy the requirements.

### 2.1 Coupling coefficients modeling

In this subsection, two kinds of the coupling coefficients, external and internal, are explained and the way to obtain two different coefficients from the simulation or measurement process with ease will be analytically given.

**Figure 1** shows an  $n$ th order filter circuit with serially connected LC resonators. The couplings between the resonators and between a resonator and input/output ports are shown with K-inverters and the values for the inverters are given using  $K_{i,j}$  and  $K_{0,1}$ , respectively. Note that the given  $n$ th order circuit consists of the serially connected resonators and impedance inverters but the identical  $n$ th order frequency response can also be realized using parallel connected LC resonators and admittance inverters. In other words, in this chapter, we extract the theoretical frequency responses using the series LC resonators with K-inverters but the same results can be obtained with parallel resonators with J-inverters due to the duality theorem.

The inverter values for the required bandpass responses can be defined as follows [3],

$$K_{0,1} = \sqrt{\frac{Z_0 L_1}{g_0 g_1}} \Delta\omega, \quad K_{i,j} = \sqrt{\frac{L_i L_j}{g_i g_j}} \Delta\omega, \quad K_{n,n+1} = \sqrt{\frac{Z_0 L_n}{g_n g_{n+1}}} \Delta\omega \quad (1)$$

where the  $\Delta\omega$  represents the bandwidth of the filter and the lowpass prototype elements are given using  $g_n$ . When the series LC resonators are replaced with generalized resonators which have the reactance slope parameter,  $x_i$ , and the inverter values given in Eq. (1) can be driven as Eq. (2),

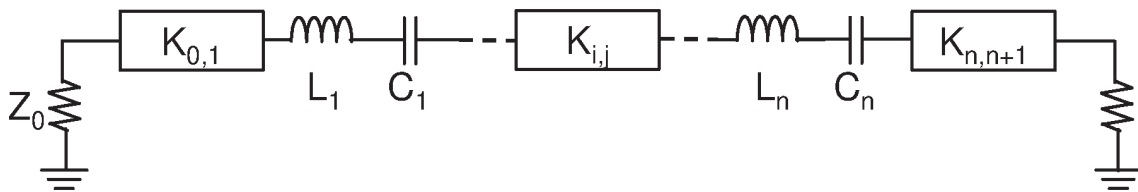


**Figure 1.**  
Nth order filter structure composed of series LC components.

$$K_{0,1} = \sqrt{\frac{Z_0 x_1}{g_0 g_1}} \text{FBW}, \quad K_{i,j} = \sqrt{\frac{x_i x_j}{g_i g_j}} \text{FBW}, \quad K_{n,n+1} = \sqrt{\frac{Z_0 x_n}{g_n g_{n+1}}} \text{FBW}. \quad (2)$$

where the FBW stands for the fractional bandwidth. In Eq. (2), port impedance  $Z_0$  can be normalized and the lowpass prototype elements, g-parameters, can be replaced using the normalized coupling coefficients,  $M_{n,n+1}$ . As a result, the K-inverter values of the  $n$ th order bandpass filter for the external and inter-resonator coupling structures are given in Eq. (3).

$$K_{0,1} = \sqrt{x_1 \text{FBW} M_{0,1}}, \quad K_{i,j} = \sqrt{x_i x_j \text{FBW} M_{i,j}}, \quad K_{n,n+1} = \sqrt{x_n \text{FBW} M_{n,n+1}}. \quad (3)$$

In a similar way, J-inverter values can be obtained with the susceptance slope parameters of parallel resonators and those are given in Eq. (4).

$$J_{0,1} = \sqrt{b_1 \text{FBW} M_{0,1}}, \quad J_{i,j} = \sqrt{b_i b_j \text{FBW} M_{i,j}}, \quad J_{n,n+1} = \sqrt{b_n \text{FBW} M_{n,n+1}}. \quad (4)$$

The theoretical frequency responses based on the normalized coupling coefficients,  $M_{n,n+1}$ , can be generated from the lowpass prototype g-parameters,  $g_n$ . **Figure 2** shows the theoretical frequency responses of the second-order filtering structures. The coupling coefficient matrices associated with the structure are given in the inset of the figures. Note that the filter can produce either bandpass or bandstop frequency response according to the coupling scheme. The theoretical responses are generated with an assumption that the filters are designed and realized with resonators having a quality factor of 350. The fractional bandwidth of the filter is set as 0.023. Note that both frequency responses are designed to have the 3-dB bandwidth at the normalized frequency of  $\omega$  is equal to 1.

In order to meet the requirement regarding the frequency response of the reconfigurable filter, the coupling structure should be designed based on the simulation or measurement process to find a suitable value for each coupling structure. With the given values for the normalized coupling coefficients and the fractional bandwidth, the inverter values for both external and internal coupling structures need to be determined to realize the required filtering responses.

**Figure 3** shows a simulation or measurement setup for the external coupling and its reflection coefficient result. The input impedance seen from the source and the reflection coefficient,  $\Gamma$ , can be given in Eq. (5).

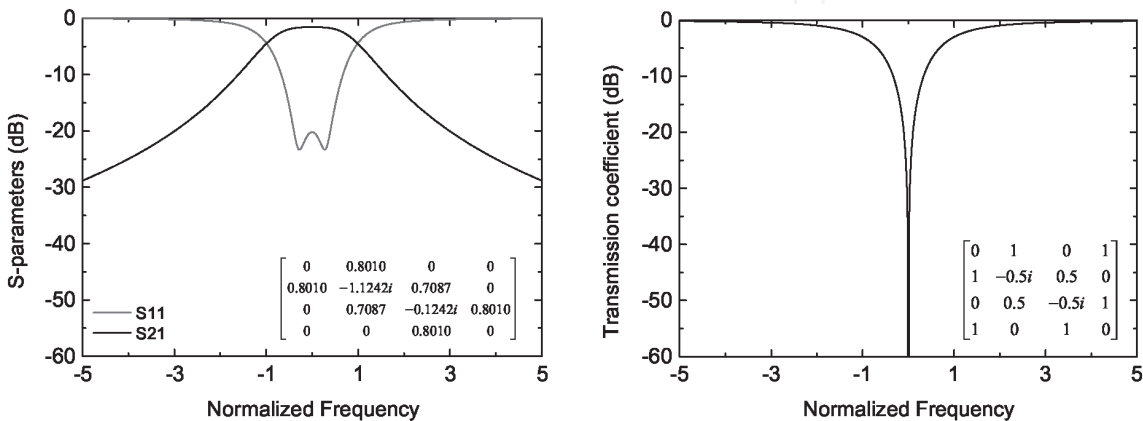


**Figure 2.**  
Theoretical frequency responses.

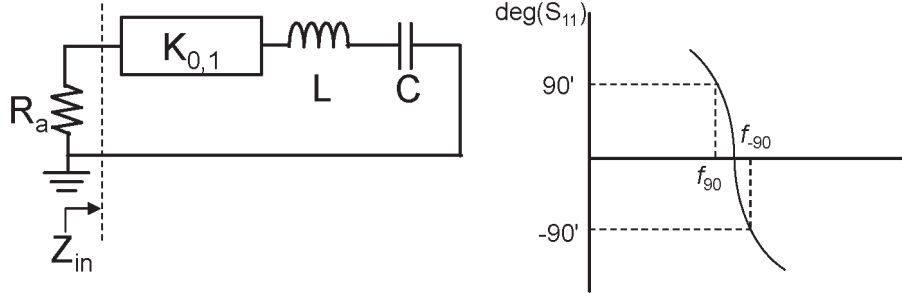


**Figure 3.** Simulation setup for an external coupling coefficient and its phase response of the reflection coefficient.

$$Z_{in} = \frac{K_{0,1}^2}{j\omega_0 L \left( \frac{\omega}{\omega_0} - \frac{\omega_0}{\omega} \right)}, \quad \Gamma = \frac{Z_{in} - R_a}{Z_{in} + R_a}. \quad (5)$$

The reflection coefficient can be reorganized with the input impedance,  $Z_{in}$ , and the frequency points at which the phase of the reflection coefficient meets  $\pm 90^\circ$ . In other words, the reflection coefficient can be organized with respect to  $\omega$  when its phase is  $90^\circ$  or  $-90^\circ$ , and two positive solutions are given in Eq. (6).

$$\omega_{+90} = \frac{-k_{01}^2 + \sqrt{k_{01}^4 + 4(R_a \omega_0 L)^2}}{2R_a L}, \quad \omega_{-90} = \frac{k_{01}^2 + \sqrt{k_{01}^4 + 4(R_a \omega_0 L)^2}}{2R_a L}. \quad (6)$$

So, the difference between two frequency points can represent the inverter value and, with the predefined form of Eq. (3), it can be summarized as Eq. (7) when the source impedance,  $R_a$ , is the same as the port impedance,  $Z_0$ .

$$f_{-90} - f_{+90} = \Delta f \cdot M_{0,1}^2. \quad (7)$$

where  $\Delta f$  is the bandwidth in Hz.

It means that the physical external coupling structure can be tuned during simulation or measurement process to meet the required design value. The design goal can be calculated with the given values such as the normalized coupling coefficient and bandwidth. As a result, the dimensions for external coupling structure can be determined or fine-tuned to achieve the prescribed frequency responses.

In addition to the external coupling structure, the reconfigurable filter also possesses the internal coupling structures and the inter-resonator coupling coefficients represent its coupling strength between resonators. **Figure 4** shows the equivalent circuit for the simulation or measurement setup for the inter-resonator coupling and its transmission coefficient result. As shown in the figure, two resonators are coupled each other through a coupling structure modeled with an inverter whose value is  $K_{ij}$ , and both resonators are fed from source or load with loosely coupled through the inverters,  $K'$  or  $K''$ . In other words, to minimize any likely effects from input and output ports given with  $Z_0$  in **Figure 4** on the inter-resonator coupling coefficients, the simulation or measurement setup for the inter-resonator coupling coefficients is designed to have small  $K'$  or  $K''$  values. The input impedance seen from the loosely coupled external ports is given in Eq. (8).

$$Z_{in} = j\omega_0 L_i \left( \frac{\omega}{\omega_0} - \frac{\omega_0}{\omega} \right) + \frac{K_{ij}^2}{j\omega_0 L_j \left( \frac{\omega}{\omega_0} - \frac{\omega_0}{\omega} \right)}. \quad (8)$$

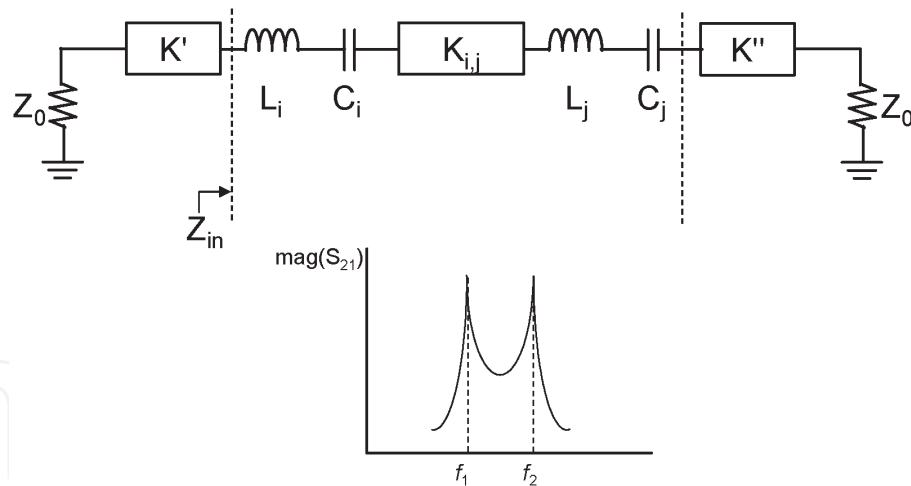


**Figure 4.**  
Simulation setup for an inter-resonator coupling coefficient and its magnitude response of the transmission coefficient.

Since two resonant peaks in the transmission response given in **Figure 4** coincide with the short-circuited frequencies, we can have frequency points by calculating its zeros of Eq. (8) with respect to the  $\omega$ . Each positive solution from two different equations can be given as  $f_1$  and  $f_2$ .

$$f_1 = \frac{-K_{ij} + \sqrt{K_{ij}^2 + 4w_0^2 L_i L_j}}{4\pi \sqrt{L_i L_j}}, \quad f_2 = \frac{K_{ij} + \sqrt{K_{ij}^2 + 4w_0^2 L_i L_j}}{4\pi \sqrt{L_i L_j}}. \quad (9)$$

Similar with the case for the external coupling coefficient design, the inter-resonator coupling coefficient can also be estimated from the distance between two frequency points and it can be calculated as Eq. (10) with the theoretical values of  $K_{ij}$  with ease.

$$f_2 - f_1 = \Delta f \cdot M_{1,2}. \quad (10)$$

Based on Eqs. (7) and (10), one can estimate the coupling structures for both external and internal couplings and precisely optimize the dimensions of structures to realize the required filter responses.

Up to this, we designed coupling structures for the external and inter-resonator couplings, and it could be done by using both theoretical responses and simulation or measurement processes. The reconfigurable characteristic can be obtained by applying the electronic components such as the varactor or pin diodes to the static coupling structures. For example, the shunt-connected varactor diodes can be embedded in the inter-resonator coupling structure and it results in different coupling coefficients comparing with the one without varactor diodes. The external coupling coefficients can also be tuned with electronic components loading to provide the proper impedance matching performance. In the following subsection, the equivalent circuits of coupling structures with tuning elements are presented in more detail.

## 2.2 Equivalent circuit modeling

In the previous subsection, the theoretical coupling values comprising a filter structure are given and simulation or measurement setup to extract the coupling coefficients is also provided. In order to realize the required filter responses with the



fabricated filter, we establish the equivalent circuits based on the theoretical values and also perform the full-wave simulation process with commercial tools such as Keysight Advanced Design System and Ansys High Frequency Structure Simulator. In this subsection, two equivalent circuits for the different frequency responses, frequency tunable bandpass and absorptive bandstop, are given to describe the operation mechanism of a reconfigurable filter [4]. Both equivalent circuits consist of the coupling structures that are covered in the previous section and those contain the electronic components to achieve the required reconfigurable characteristic. During the simulation, the capability of loaded electronic components that change the coupling coefficients can be figured out and the detailed simulation results are given in [4].

**Figure 5** shows an equivalent circuit for a frequency tunable two-pole bandpass response. It contains two LC resonators coupled each other through an iris which is modeled using an inductor,  $L_c$ . A short-circuited microstrip line with shunt connected capacitors also contributes the inter-resonator coupling at the same time. The input and output lines are also coupled to the resonators. As mentioned in the previous section, the reconfigurable characteristics can be realized by tuning the coupling structures and, in this equivalent circuit, the short-circuited capacitors,  $C_i$  and  $C_e$ , are placed to optimize the internal and external coupling coefficients, respectively. The operating frequency agility is basically achieved by changing the value of  $C_r$  and the passband bandwidth can mainly be tuned by  $C_i$ . A capacitor serially shunt-connected to the input and output port using a short length of microstrip line ( $l_m$ ) can control the matching performance. As a result, all features for the bandpass frequency responses can be controlled with three different capacitors.

**Figure 6** shows the simulation results for the operating and bandwidth tuning performance of the bandpass equivalent circuit. The detailed circuit parameters can

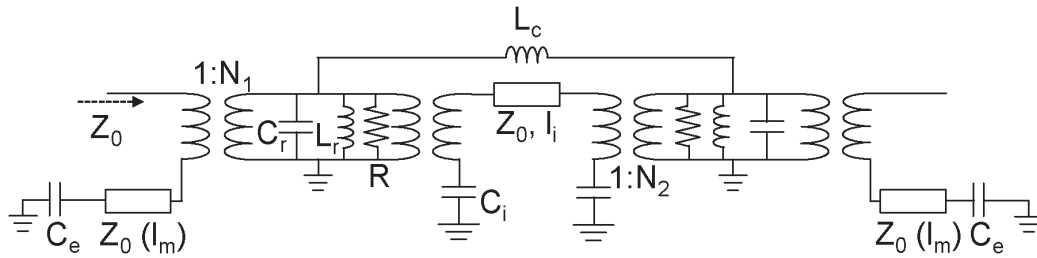


**Figure 5.**  
Equivalent circuit for bandpass frequency response of the reconfigurable filter.

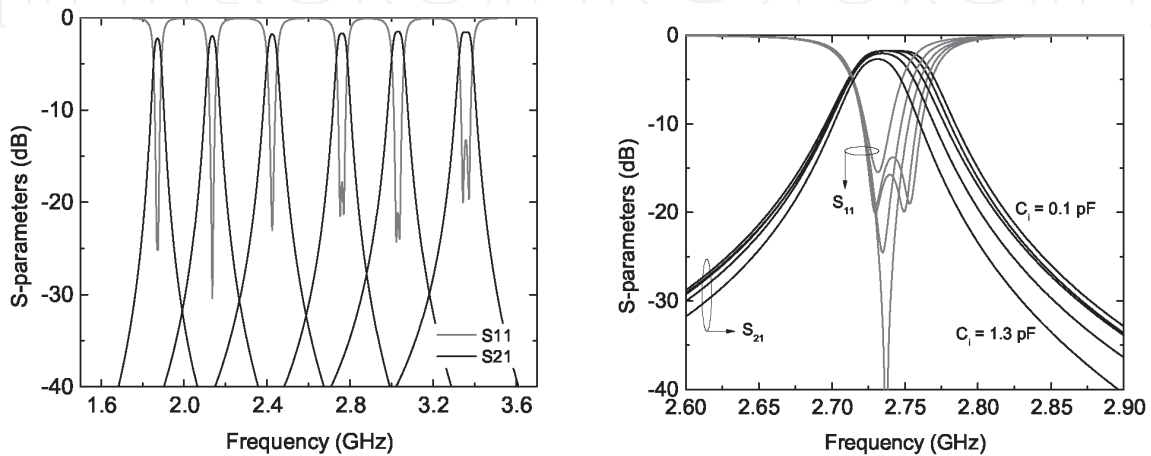


**Figure 6.**  
Simulation results for the operating frequency and bandwidth tuning performance of the bandpass equivalent circuit.

be initially decided when the coupling structures for external and inter-resonator couplings are investigated using the full-wave simulation process as given in the previous section. The initial circuit parameters except for the three capacitance values are  $N_1 = 1.05$ ,  $N_2 = 2.2$ ,  $l_m = 0.357$  in,  $l_i = 0.315$  in,  $L_r = 10.467$  nH and  $L_c = 6.978$  nH. The capacitance for resonators  $C_r$  is used from 22 pF to 70 pF and the other two capacitance values are determined based on the reasonable values from the commercial varactor diodes. The frequency tuning ratio of larger than 1.7:1 is expected based on the simulation results. The different capacitance loading  $C_i$  changes the resonant frequency of a resonant mode so it results in the bandwidth control capability. Note that the simulation for the bandwidth tuning is performed with a fixed  $C_r$  value and the similar tuning performance can be obtained over the frequency tuning range of interest. The simulation results exhibit that one can tune the center frequency and bandwidth of the filter maintaining the impedance matching performance.

**Figure 7** shows the equivalent circuit for the absorptive bandstop frequency response. Similar to the one for the bandpass frequency response it can change the operating frequency by changing the capacitance which is the part of resonators. In order to realize the unity coupling value between source and load as given in the inset of the theoretical frequency response, the microstrip line which is designed to have an electrical length of  $270^\circ$  at 2.2 GHz is added between two ports. Except for the microstrip line for  $M_{sl}$ , the rest of the circuit parameters are the same as those for the bandpass mode equivalent circuit. The absorptive frequency responses given in **Figure 8** can be characterized with the reduced reflection coefficients at the stopband of the bandstop filtering response. The equivalent circuit shows the best absorptive characteristic at 2.2 GHz of the predetermined center frequency but the amount of the reflection coefficient increases as the operating frequency is tuned from the predetermined one since the electrical length of the microstrip line deviates from the center frequency. In other words, the frequency tuning range of the absorptive bandstop mode is mainly limited by the electrical length of the filter structures and, in this case, it is about 500 MHz with less than  $-10$  dB reflection coefficient.

Two equivalent circuits shown in **Figures 5** and **7** are realized using frequency tunable substrate integrated waveguide (SIW) resonators, varactor diodes, and single pole double throw (SPDT) switches. Two frequency tunable resonators and the microstrip line structure are placed at the different substrate and are coupled through coupling slots. The commercial varactor diodes are embedded in the microstrip line and are used to tune the coupling strength with different input voltages. In order to realize both bandpass and absorptive bandstop responses using a filter structure, two SPDT switches are also embedded in the microstrip line designed to provide  $M_{sl}$  coupling between source and load.

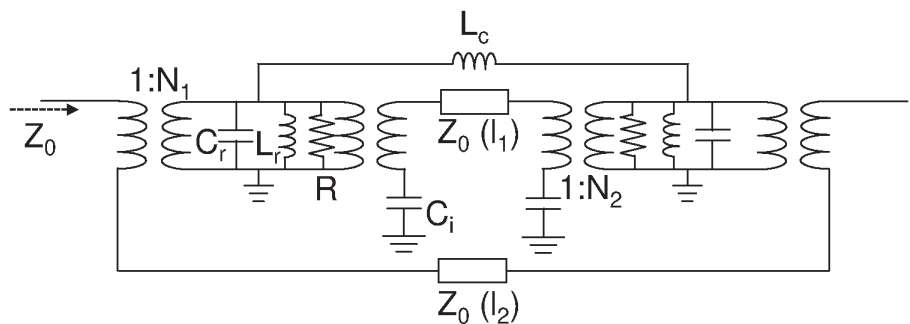


**Figure 7.**  
Equivalent circuit for absorptive bandstop frequency response of the reconfigurable filter.



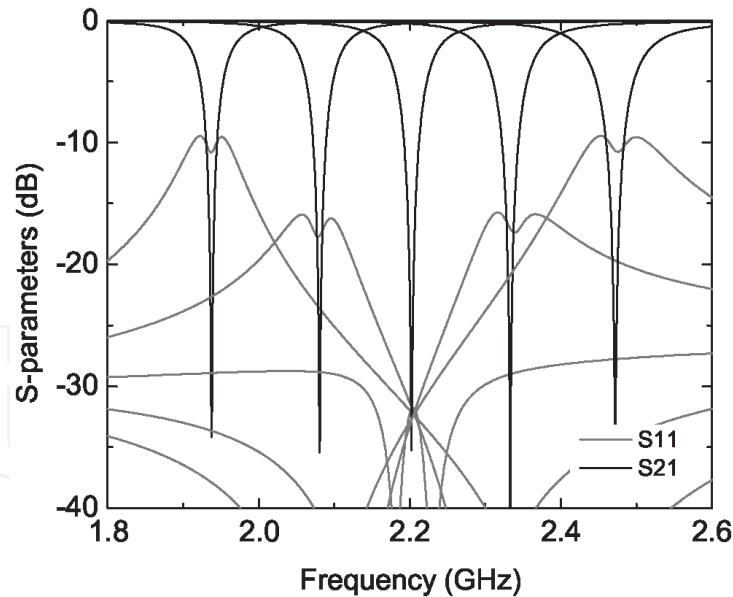


**Figure 8.**  
*Simulation results of the equivalent circuit for the absorptive bandstop responses.*

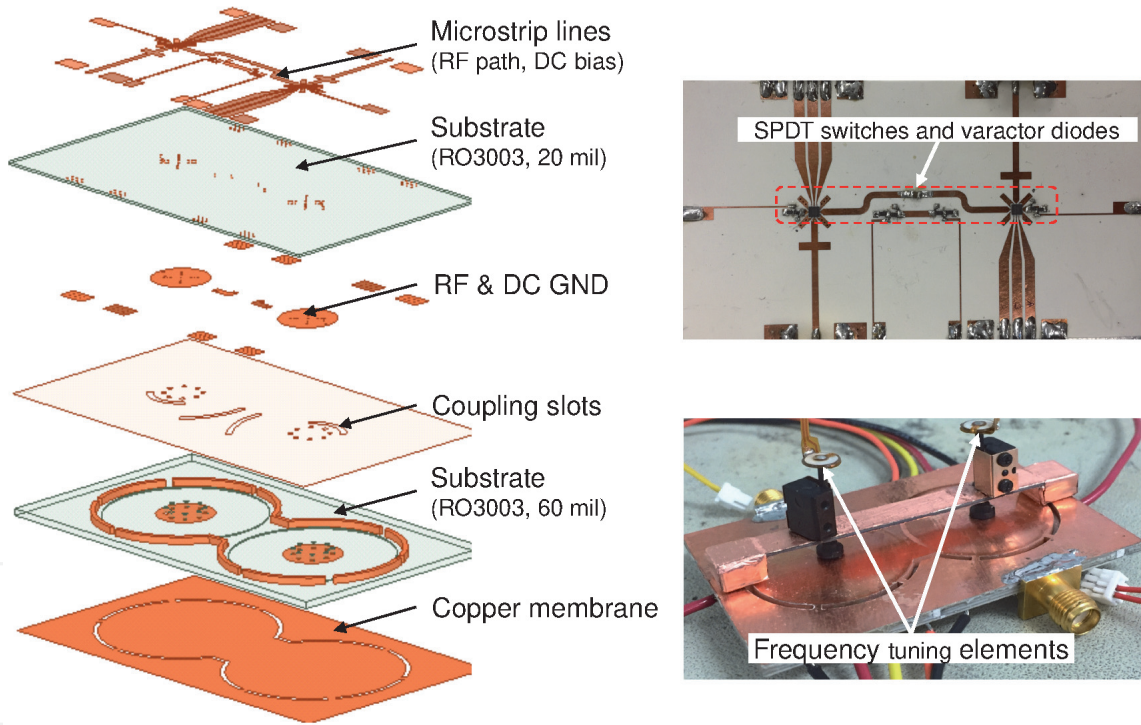


**Figure 9.**  
*Reconfigurable filter configuration and a photograph of the filter with frequency tuning elements.*

**2.3 SIW resonator-based reconfigurable filter**

**Figure 9** shows the filter configuration and a photograph of the fabricated filter with two frequency tuning elements [4]. At the top of the fabricated circuit, the microstrip line for the RF input signal is etched together with direct current (DC) bias lines for the electronic components. The coupling slots in the ground plane of the microstrip line are used to control the external or internal coupling and their size should be optimized in order to satisfy both bandpass and absorptive bandstop frequency responses. In virtue of the shunt-connected varactor diodes embedded in the microstrip, one can realize or achieve the coupling coefficient requirement over the frequency tuning range of interest. The SIW resonator consists of conductive

posts at the center of the resonator and, with a copper membrane attached at the bottom of the resonator, high capacitance is loaded between the copper membrane and a circular-shaped ground plane of the post. The frequency agility is achieved by changing the loaded capacitance, and it means that the thickness of the air gap determines the resonant frequency of the frequency tunable SIW resonator. The frequency tuning elements attached at the bottom of the resonator are designed to change the air-gap thickness with the movement of a shaft connected to a piezoelectric disk actuator. More about the tuning element will be given in the next section.

**Figure 10** shows the measurement results of the bandpass mode of the reconfigurable filter. The operating frequency is tuned from 1.86 to 3.3 GHz. The resonant frequency is tuned using two piezo disk-based tuning elements and the impedance matching performance of at least below  $-10$  dB reflection coefficient is maintained over the frequency tuning range thanks to the varactor diodes for the external coupling optimization. As shown in the frequency tuning measurement results, the filter exhibits the different passband bandwidth as its operating frequency is tuned. Since the coupling strength generated from the coupling slots is unavoidably frequency dependent, so the coupling coefficient from a coupling slot with a fixed dimension can be different as the operating frequency of the filter is tuned. As mentioned earlier, the passband bandwidth is mainly controlled with the varactor diodes which have a capacitance value of  $C_i$  in **Figure 5**. The fabricated filter can also maintain its passband bandwidth even though the operating frequency is changed. In the right graph of **Figure 10**, the capacitance values are set to realize 80 MHz constant bandwidth with about 640 MHz frequency tuning range. **Figure 11** shows the measurement results of the absorptive bandstop mode of the fabricated filter. As expected from the simulation result given in **Figure 8**, the absorptive characteristic is maintained over the frequency tuning range of interest and the amount of reflection coefficient and attenuation performance get worse when the operation frequency moves away from the frequency where the  $l_2$  given in **Figure 7** satisfies the electrical length of  $270^\circ$ . The fabricated filter provides more than 500 MHz of frequency tuning range when it operates as an absorptive bandstop mode.

In the following section, the frequency tuning elements that can be applied to the aforementioned frequency tunable SIW resonators will be given. First, the piezoelectric disk-based tiny ultra-linear actuator will be introduced with its detailed operating mechanism and then we will provide the recently proposed tuning method based on the magnetically actuated tuning elements. Finally, a filtering balun structure is fabricated and its frequency tunable characteristic is tested using four electromagnets to verify the proposed magnetically actuated tuning method.

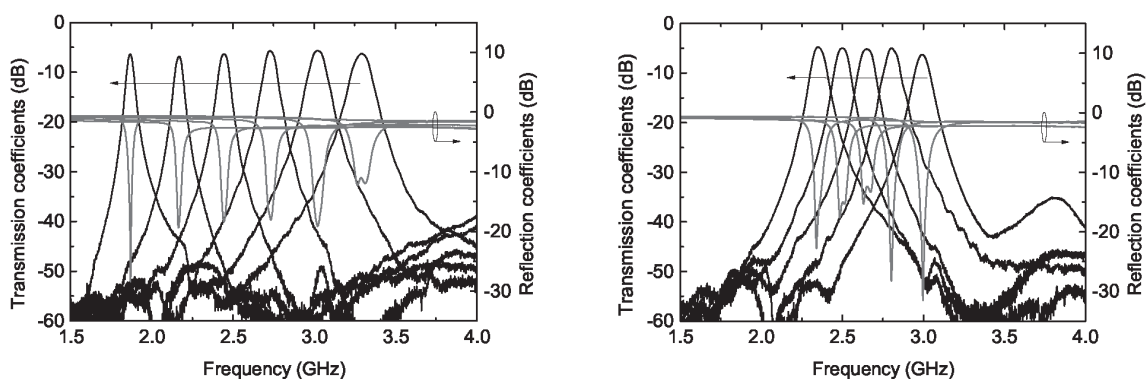


**Figure 10.**  
 Measured bandpass mode frequency responses.

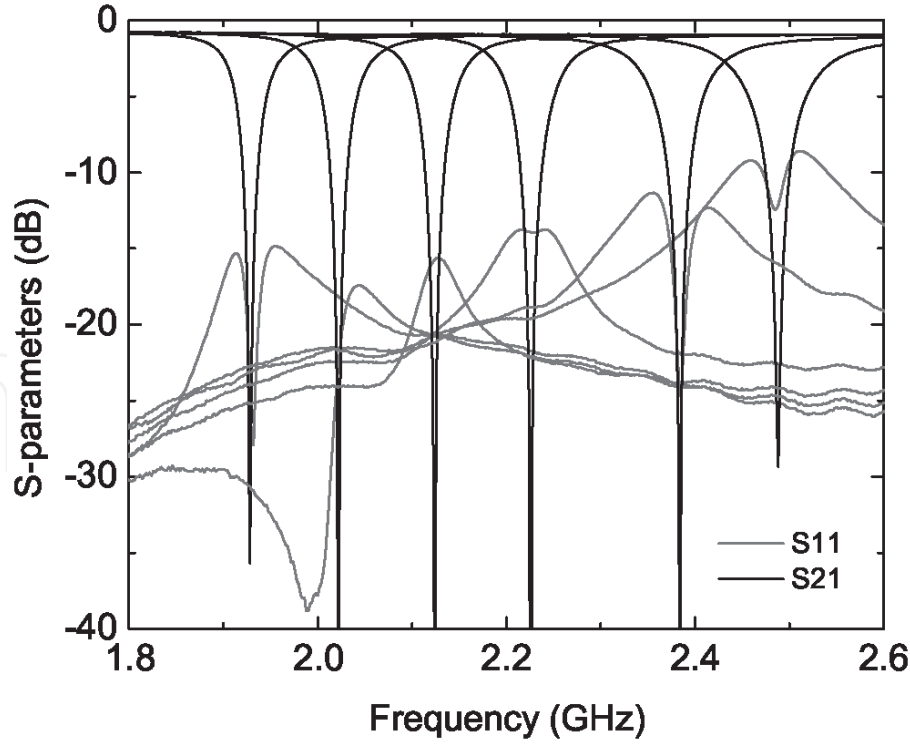


**Figure 11.**  
Measured absorptive bandstop mode frequency responses.

### 3. Frequency tuning elements

In order to achieve frequency agility, one can exploit the tuning elements in the filter structures. Those can be varactor or pin diodes when the filters are designed with lumped or distributed elements such as microstrip lines since they can change and perturb the electrical length or the electromagnetic fields in the structures [5]. In this section, two different kinds of frequency tuning elements and their application to the frequency tunable substrate integrated waveguide resonator will be covered.

#### 3.1 Piezoelectric disk-based elements

The frequency tunable SIW resonator shown in the previous section utilizes a piezoelectric disk-based actuator to change the thickness of an air gap in which the electric field is strong [6]. The piezoelectric actuator can be applied to the SIW resonator in two different ways.

Firstly, as shown in [6], the piezo disks can be directly attached to the copper membrane and react to the applied DC voltage. The thickness of the disk can be varied with the applied voltage so the different air-gap thicknesses result in the resonant frequency tuning. However, there are two drawbacks in directly attaching the piezo disk to the resonators. One is the size of the disk itself as it should cover the whole of the copper membrane and supporting substrate to properly operate its function and it can limit the size of the resonator as well. It means that the piezo disk may not be large enough to cover the frequency tunable resonator designed to operate at lower frequency bands. The second drawback is the large input voltage range with the hysteresis effects. The applied input voltage is dependent on the piezo disks, but it could be from  $-200$  to  $+200$  V to satisfy the sufficient frequency tuning range requirements. In addition, the amount of changes in the thickness is not identical when the applied voltage moves from low to high level or from low to high level due to the hysteresis effect.

Secondly, the frequency tunable substrate integrated waveguide resonator utilizes the tiny ultra-linear actuators, named TULA to tune the resonant frequency [7]. The devised element shown in **Figure 12** is comprised of a small piezo disk with a post attached to and the input voltage is applied by using a small driver circuit that can be controlled with commercial software. The applied voltage pulse has a form of sawtooth and the post attached to the piezo disk moves upward or downward. The reported linear actuator has an advantage over the disk type of piezoelectric actuator as it can provide a predictable amount of movement per the amplitude of pulse in spite of the hysteresis of the piezo disk. But these tuning elements can limit the filter to be assembled with a neighboring circuit due to the size of the fixture with a shaft. In addition, one end of the post should be glued to the copper membrane to control the air-gap thickness, so during the fabrication process, especially in the attachment of the post to the filter, there is a chance of serious damage to the copper membrane. In addition, it is not a practical way to realize the frequency tunable characteristic when low cost, compact volume designs are needed.

3.2 Magnetically actuated tuning elements

In this subsection, a recently reported frequency tuning method that can be applied to the frequency tunable substrate integrated waveguide resonators will be covered [8]. An electromagnet with a high permeability foil are utilized to tune the resonant frequency without any contacts between the resonators and tuning elements. A foil sheet is glued on the copper membrane during the fabrication process so the thickness of an air gap can be tuned with the applied magnetic flux from the electromagnet. Based on this method, the resonant frequency of the filter can be precisely tuned and the copper membrane can maintain its status as it was fabricated since the frequency tuning element, electromagnet, does not contact the filter circuit, unlike the piezoelectric actuator. A detailed explanation along with the simulation and measurement results is given in the following.

**Figure 13** shows simplified 3D and side view of the circular-shaped substrate integrated waveguide resonator. A copper plate is circularly etched at the bottom of the substrate and is also electrically connected to the top plate via conductive via-holes. A large amount of capacitance is generated at the air gap between the copper

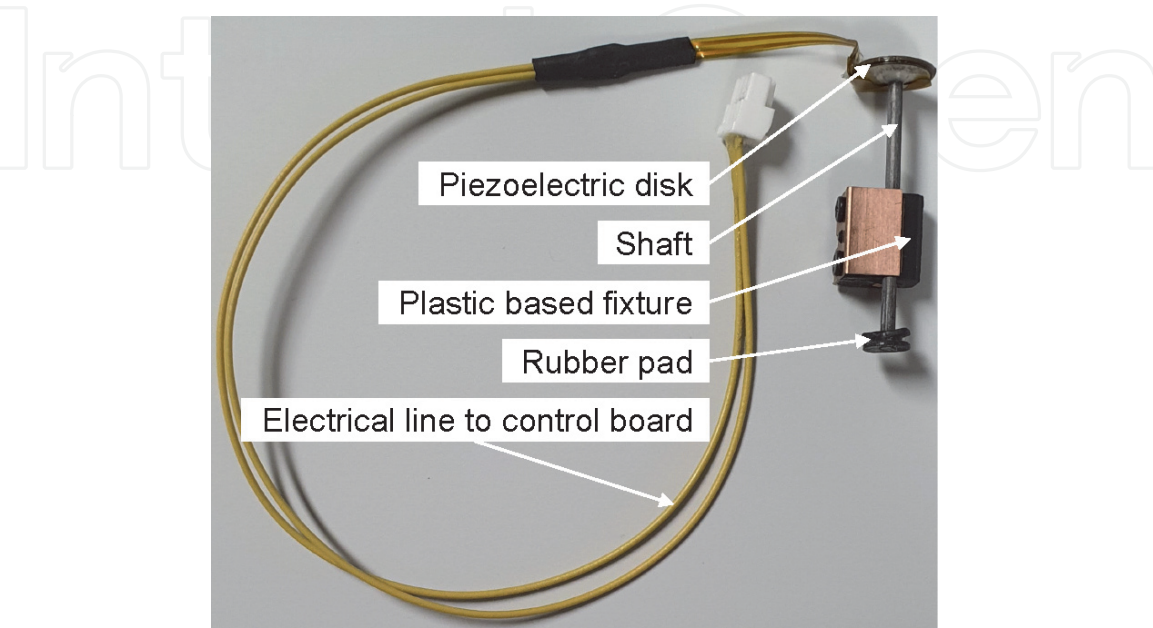


**Figure 12.**  
*A photograph of a piezoelectric disk-based tiny ultra-linear actuator.*



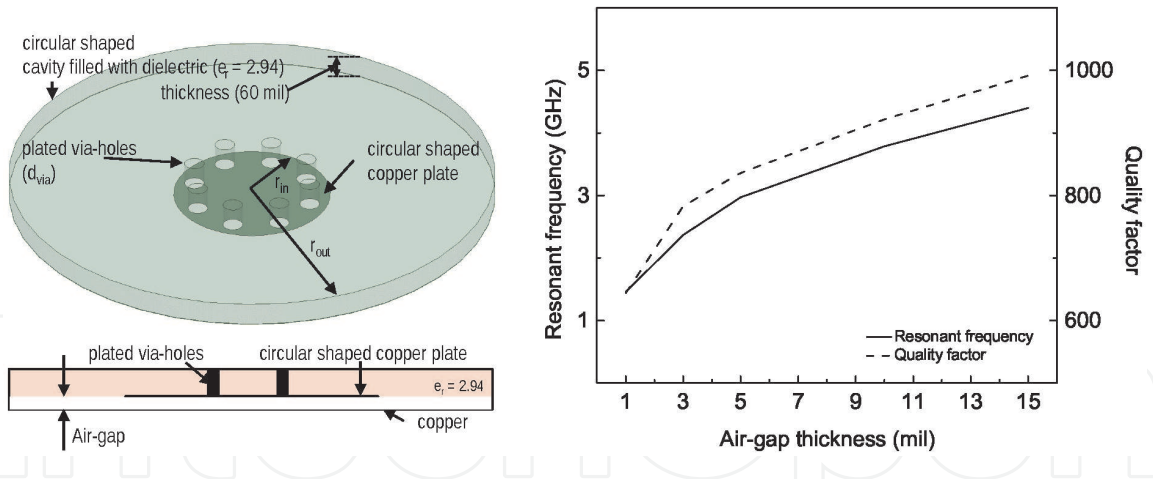


**Figure 13.** Simplified view of a frequency tunable circular SIW resonator and its electrical characteristics.

plate and the copper membrane so the resonant frequency tuning mainly can be done by changing the thickness of an air gap. The relationship between the thickness and resonant frequency as well as the quality factor is simulated and the results are also given in **Figure 13**.

Based on the Eigen model simulation results, a single-frequency tunable resonator is designed to support the electromagnet-based tuning method. As shown in the upper left figure of **Figure 14**, two conductor-backed coplanar waveguide lines which are designed to have  $50 \Omega$  characteristic impedance are used as input and output lines. Two radial-shaped slots control the external couplings between  $50 \Omega$  line and resonator so a tight coupling can be achieved with a larger coupling slot. The side view is also given for the fabrication process, and it is noted that a high permeability foil is glued at the bottom of the resonator with the same adhesive used for the lamination of two substrates. The photograph of a fabricated resonator with a high permeability foil is also shown in **Figure 14**. The high permeability sheet glued to the frequency tunable SIW resonator for the magnetically actuated tuning method is from Metglas, Inc.

Prior to the implementation of the proposed frequency tuning method to the fabricated filter structure, the magnetic flux density and the current consumption from an electromagnet need to be investigated and the measured results are given in **Figure 15**. The magnetic flux density is measured using a Tesla meter and a probe as

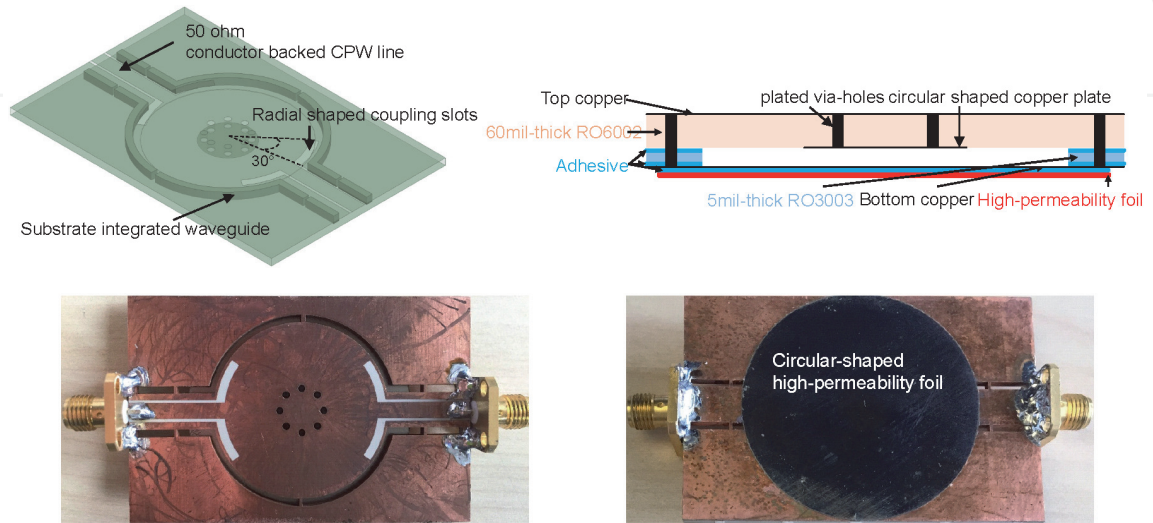


**Figure 14.** Simulation model of frequency tunable SIW resonator, a side view drawing of the fabricated circuit, and photographs of SIW resonator.



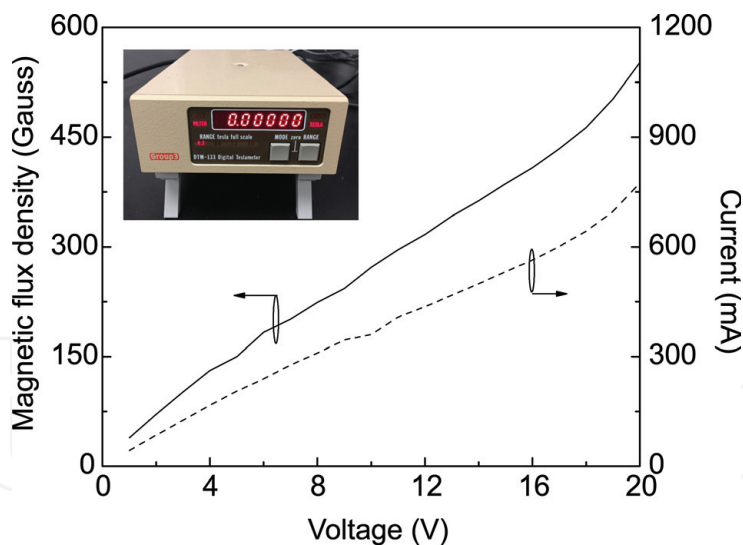


**Figure 15.**  
*Measured magnetic flux density and current consumption from an electromagnet.*

shown in the inset of **Figure 15**. An electromagnet used for the measurement is a readily available one from market and its rated input voltage is 12 V, so applying the input voltage larger than the rated voltage for a long period of time can result in a damage of the electromagnet.

The electromagnet is placed both upper and lower sides of the fabricated one-pole frequency tunable SIW resonator to tune the resonant frequency as shown in **Figure 16**. Since the electromagnet only generates an attraction force from the input voltage, two electromagnets are used to move the high permeability foil in the opposite direction. In order to maximize the frequency tuning range, the input voltage to the electromagnet is applied to each at a time. The resonant frequency is tuned from 1.3 to 3.7 GHz which is larger than the frequency tuning ratio of 2.8:1.

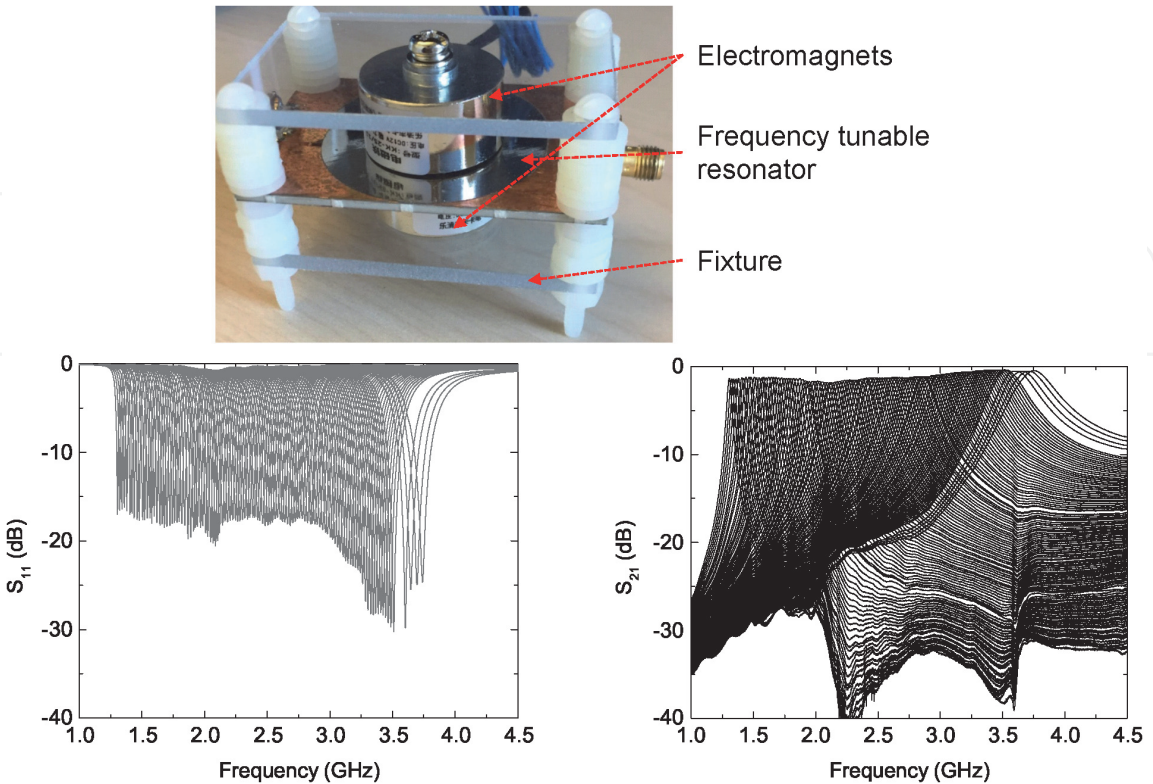


**Figure 16.**  
*Photograph of the fabricated one-pole frequency tunable SIW resonator with electromagnets and its measured frequency responses.*

In future research on the magnetically actuated tuning elements, the smaller electromagnetic that can generate two-way magnetic forces with lower input voltage to satisfy the specific applications are expected.

3.3 Frequency tunable filtering balun with magnetically actuated tuning method

In this subsection, a filtering balun design is provided and its resonant frequency is tuned based on the aforementioned magnetically actuated tuning method. The fundamental design theory for the frequency tunable filtering balun follows the one reported in [9] except for the order of circuit structure and the required frequency tuning range.

**Figure 17** shows the exploded view of the frequency tunable filtering balun. Similar to the reconfigurable filter given in [8], the filtering balun consists of two different substrates and each substrate contains the microstrip lines or SIW resonators, respectively. The couplings between two substrates are achieved through coupling slots placed at the ground plane of the microstrip line. To meet the requirement of balun, one port is designed in form of a single-ended microstrip input line and the other two ports have differential output lines. The short-circuited microstrip line fed the SIW resonator and the two ports connected to the other microstrip line receive output signal having an equal magnitude and a phase difference of 180°. This can be done by introducing a coupling slot at the center of the U-shaped microstrip [9]. As shown in the photograph of the fabricated filtering balun, two circular-shaped foils which have a high permeability are glued at the bottom of the devised circuit. Two electromagnets are placed at both sides of the circuit for each frequency tunable SIW resonator. To satisfy the required frequency tuning range, the electromagnets are placed as close as possible by optimizing the height of the plastic support. The electromagnets are the same as those used in **Figure 16**, so the input voltage can also be swept from 0 V to 12 V.

**Figure 19** presents the simulation results of the filtering balun. The required frequency tuning is about 17% at the center frequency of 2.9 GHz with the proper performance on the differential output line such as the amplitude and phased imbalance. The mixed-mode S-parameters ( $S_{ds21}$ ,  $S_{cs21}$ , and  $S_{dd22}$ ) are calculated and

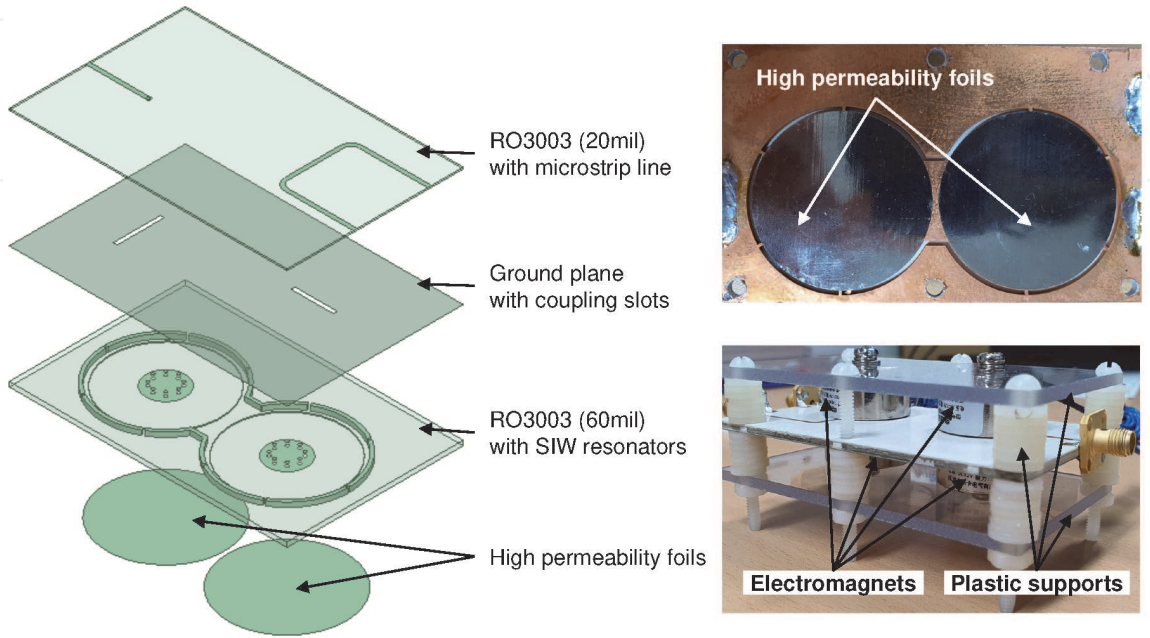


**Figure 17.** Simulation model of the frequency tunable filtering balun and its detailed view with high permeability foils.

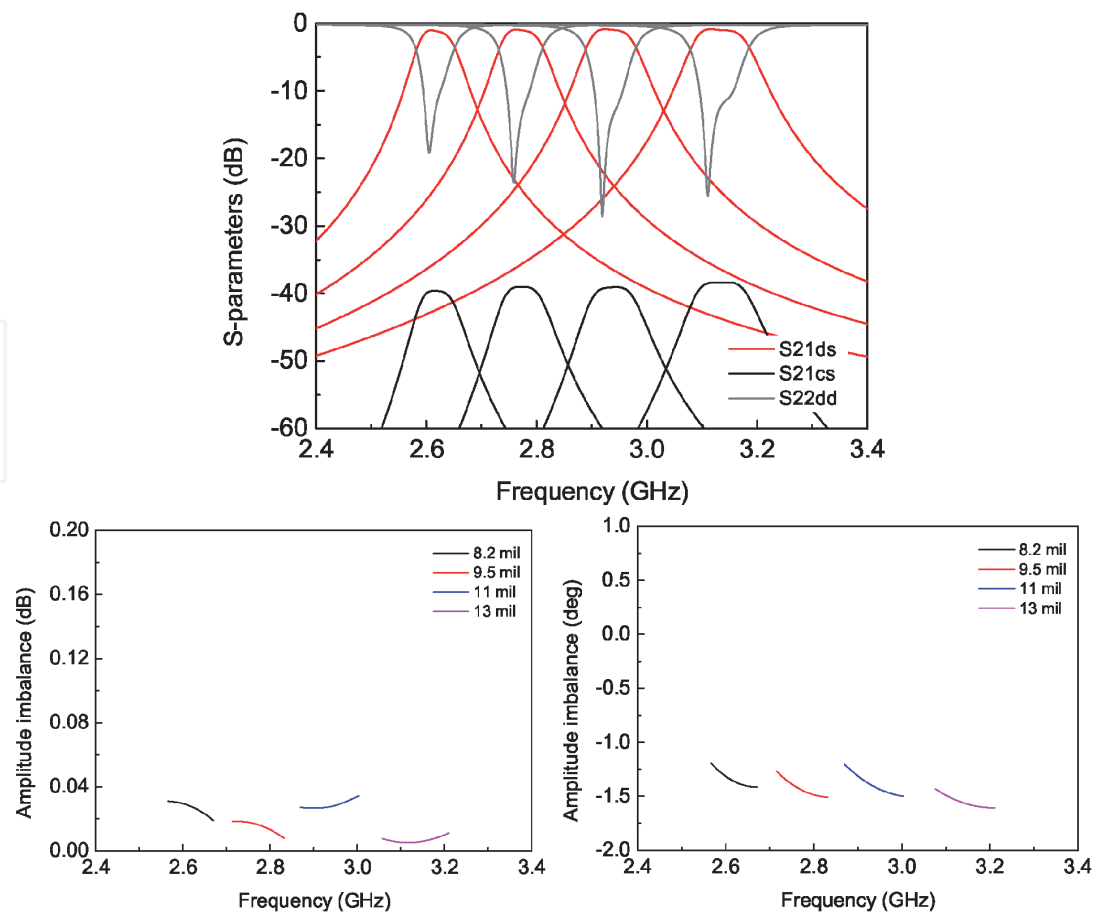


**Figure 18.**  
*Simulation results of the frequency tunable filtering balun.*

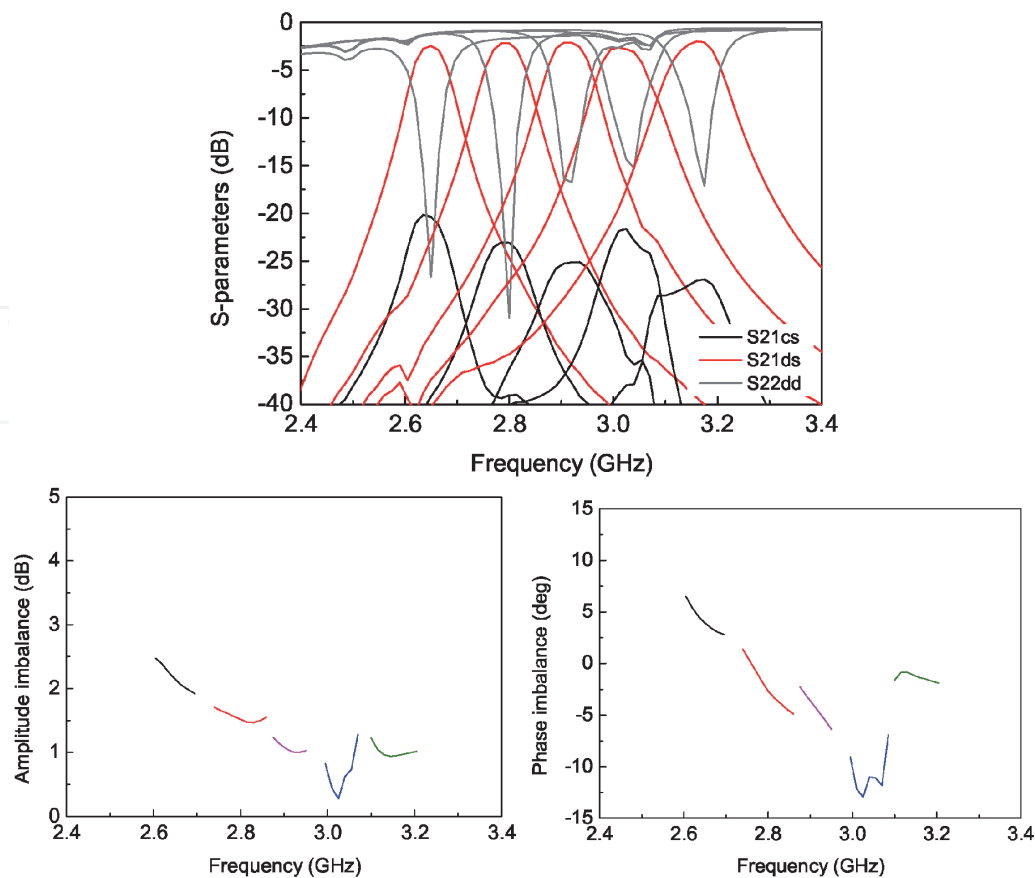


**Figure 19.**  
*Measurement results of the frequency tunable filtering balun.*

also given in **Figures 18 and 19**. The operating frequency of the fabricated filtering balun is tuned from 2.65 to 3.15 GHz which satisfies the requirement and both amplitude and phase imbalanced performance at the passbands are given. Some discrepancies between the simulated and measured results are from some unexpected factors raised from fabrication or assemblies that can impact the electrical characteristic of the differential output signal. In this section, the frequency tuning method utilizing the electromagnets with high-permeability foil has been tested and the measurement results show that it can provide a comparable performance with the one with piezoelectric disks.

#### **4. Conclusions**

In this chapter, we explore the design process of the reconfigurable filter which can exhibit both frequency tunable bandpass and absorptive bandstop frequency responses. The coupling structures that can satisfy the predetermined requirements are designed from the theoretical normalized coupling coefficients, and its simulation/measurement models are also given. In order to realize the frequency tunable characteristic, two different tuning elements which are based on the piezoelectric disks or electromagnets are shown with the operation mechanism, and its application to the fabricated filtering balun is implemented especially using the electromagnets.

#### **Acknowledgements**

The authors want to thank Mr. Traian Antonescu and Mr. Steve Dubé from Ecole Polytechnique, PolyGrames Research Center for their professional fabrication.

#### **Author details**

Tae-Hak Lee<sup>1\*</sup>, Sang-Gyu Lee<sup>2</sup>, Jean-Jacques Laurin<sup>3</sup> and Ke Wu<sup>3</sup>


<sup>1</sup> Yuhan University, Department of Electronic Engineering, Bucheon, Republic of Korea

<sup>2</sup> Korea Aerospace Research Institute, Satellite Payload Research and Development Division, Daejeon, Republic of Korea

<sup>3</sup> PolyGrames Research Center, École Polytechnique (Montréal University), Montréal, QC, Canada

\*Address all correspondence to: taehaklee@gmail.com

#### **IntechOpen**

© 2021 The Author(s). Licensee IntechOpen. This chapter is distributed under the terms of the Creative Commons Attribution License (<http://creativecommons.org/licenses/by/3.0>), which permits unrestricted use, distribution, and reproduction in any medium, provided the original work is properly cited. 



## References

- [1] Cameron RJ, Kudsia CM, Mansour RR. *Microwave Filters for Communication Systems: Fundamentals, Design, and Application*. 2nd ed. Hoboken: Wiley; 2018. DOI: 10.1002/9781119292371
- [2] Hong JS. *Microstrip Filters for RF/Microwave Applications*. 2nd ed. New York: Wiley; 2011. DOI: 10.1002/9780470937297
- [3] Matthaei G, Jones EMT, Young L. *Microwave Filters, Impedance Matching Networks, and Coupling Structures*. Norwood: Artech House; 1980
- [4] Lee T-H, Laurin J-J, Wu K. Reconfigurable filter for bandpass-to-absorptive bandstop responses. *IEEE Access*. 2020;8:6484-6495. DOI: 10.1109/ACCESS.2019.2963710
- [5] Yang T, Rebeiz GM. Bandpass-to-bandstop reconfigurable tunable filters with frequency and bandwidth controls. *IEEE Transaction on Microwave Theory and Technology*. 2017;65:2288-2297. DOI: 10.1109/TMTT.2017.2679182
- [6] Moon S, Sigmarsson HH, Joshi H, Chappell WJ. Substrate integrated evanescent mode cavity filter with a 3.5 to 1 tuning ratio. *IEEE Microwave Wireless Components Letters*. 2010;20:450-452. DOI: 10.1109/LMWC.2010.2050680
- [7] Lee B, Nam S, Lee T-H, Ahn C-S, Lee J. Single-filter structure with tunable operating frequency in noncontiguous bands. *IEEE Transactions on Components, Packaging and Manufacturing Technology*. 2017;7:98-105. DOI: 10.1109/TCPMT.2016.2623804
- [8] Lee T-H, Laurin J-J, Wu K. A wideband frequency-tuning method using magnetically actuated mechanical tuning of a SIW resonator. In: *Proceedings of the IEEE International Microwave Conference (IMS 2019)*; 1-7 June 2019; Boston. MA: IEEE; 2019. pp. 1-4
- [9] Hickie MD, Peroulis D. A widely-tunable substrate-integrated balun filter. In: *Proceedings of the IEEE International Microwave Conference (IMS 2017)*; 4-9 June 2017; Honolulu. HI: IEEE; 2017. pp. 1-4